atmosphere

MDPI

Review

Estimation of Atmospheric Fossil Fuel CO_2 Traced by $\Delta^{14}C$: Current Status and Outlook

Ming-Yuan Yu [1,2], Yu-Chi Lin [1,2] and Yan-Lin Zhang [1,2,*]

[1] School of Applied Meteorology, Nanjing University of Information Science and Technology, Nanjing 210044, China
[2] Atmospheric Environment Center, Joint Laboratory for International Cooperation on Climate and Environmental Change, Ministry of Education, Nanjing University of Information Science and Technology, Nanjing 210044, China
* Correspondence: zhangyanlin@nuist.edu.cn

Abstract: Fossil fuel carbon dioxide ($FFCO_2$) is a major source of atmospheric greenhouse gases that result in global climate change. Quantification of the atmospheric concentrations and emissions of $FFCO_2$ is of vital importance to understand its environmental process and to formulate and evaluate the efficiency of carbon emission reduction strategies. Focusing on this topic, we summarized the state-of-the-art method to trace $FFCO_2$ using radiocarbon (^{14}C), and reviewed the $^{14}CO_2$ measurements and the calculated $FFCO_2$ concentrations conducted in the last two decades. With the mapped-out spatial distribution of $^{14}CO_2$ values, the typical regional distribution patterns and their driving factors are discussed. The global distribution of $FFCO_2$ concentrations is also presented, and the datasets are far fewer than $^{14}CO_2$ measurements. With the combination of ^{14}C measurements and atmospheric transport models, the $FFCO_2$ concentration and its cross-regional transport can be well interpreted. Recent progress in inverse methods can further constrain emission inventories well, providing an independent verification method for emission control strategies. This article reviewed the latest developments in the estimation of $FFCO_2$ and discussed the urgent requirements for the control of $FFCO_2$ according to the current situation of climate change.

Keywords: radiocarbon; fossil fuel carbon dioxide; emission estimation; carbon emission reduction

Citation: Yu, M.-Y.; Lin, Y.-C.; Zhang, Y.-L. Estimation of Atmospheric Fossil Fuel CO_2 Traced by $\Delta^{14}C$: Current Status and Outlook. *Atmosphere* **2022**, *13*, 2131. https://doi.org/10.3390/atmos13122131

Academic Editor: Jaroslaw Krzywanski

Received: 25 November 2022
Accepted: 15 December 2022
Published: 19 December 2022

1. Introduction

Carbon dioxide (CO_2), the most important greenhouse gas, is a significant driver of global warming. In 2019, the annual average concentration of CO_2 reached 410 ppm, which was higher than any time in at least 2 million years [1]. The observed increase in CO_2 concentrations since the beginning of the industrial era is unequivocally caused by human activities, among which the combustion of fossil fuels is responsible for most of the total anthropogenic CO_2 emissions. Global warming has caused increases in the global temperature of the surface and upper ocean, increases in precipitation and sea level, weather, and climate extremes, and decreases in glaciers and sea ice [2–5]. Besides CO_2, fossil fuel combustion is also a primary contributor to air pollutants [6]. Thus, slowing down the increase in fossil fuel CO_2 ($FFCO_2$) concentration is of vital importance. According to the Paris Agreement and the sixth assessment report of IPCC (Intergovernmental Panel on Climate Change), CO_2 emissions need to be net negative to hold the global surface temperature lower than 1.5 °C or 2 °C at the end of this century (very low and low greenhouse gas emission scenarios, according to IPCC, 2021). This means that the anthropogenic removal of CO_2 exceed anthropogenic emissions. Under these circumstances, identifying the contribution of $FFCO_2$ to total atmospheric CO_2, as well as its atmospheric process interpretation and emission estimation, is a fundamental work for studies on its climatic and environmental impacts and on the evaluation of mitigation actions.

Multiple tracers that co-emitted with CO_2 have been used to quantify $FFCO_2$, including carbon monoxide (CO), sulfur hexafluoride (SF_6), tetrachloroethylene (C_2Cl_4) and even air pollutants, based on the ratio of each tracer to CO_2 [7–14]. However, there are large uncertainties due to the non-fossil emissions of the tracers [15]. Radiocarbon (^{14}C), a widely used dating method in archaeology, geosciences, etc. [16], is a direct tracer and a promising method to differentiate the emissions of fossil fuel and non-fossil fuel from atmospheric carbon. The abundances of three naturally occurring carbon isotopes ^{12}C, ^{13}C and ^{14}C are 98.89%, 1.11%, and ~10^{-10}%, respectively [17]. The radiocarbon content of CO_2 is expressed as $\Delta^{14}C$ or $\Delta^{14}CO_2$ [18,19]:

$$\Delta^{14}C = \left[\frac{(^{14}C/^{12}C)_{SN}}{(^{14}C/^{12}C)_{ABS}} - 1 \right] \times 1000‰. \quad (1)$$

$(^{14}C/^{12}C)_{SN}$ is the ^{14}C to ^{12}C ratio of the sample, and $(^{14}C/^{12}C)_{ABS}$ is related to the commonly used primary measurement standard Oxalic Acid I. Radiocarbon is cosmogenic, and has a radioactive half-life of 5730 ± 40 years [20]. Thus, there are no ^{14}C in fossil fuels because they are all depleted during long-term radioactive decay. Since fossil fuel CO_2 contains no ^{14}C whereas CO_2 from other sources has similar ^{14}C concentrations with the ambient air, the release of fossil fuel CO_2 will cause a decrease in the $^{14}C/^{12}C$ ratio in the atmosphere. This was first discovered by Hans Suess [21], and is called the "Suess effect". With industrial development, atmospheric $\Delta^{14}CO_2$ decreased by 25‰ between 1890 and 1950 [22]. Then comes the nuclear testing period between the 1950s and the early 1960s, during which large-scale detonations of nuclear bombs produced ^{14}C atoms in the Northern Hemisphere. Atmospheric $\Delta^{14}CO_2$ in the Northern Hemisphere increased swiftly and reached a peak value of nearly 1000‰ in 1963, and then decreased after the Limited Nuclear Test Ban Treaty [23,24]. In addition to those mentioned above, other principal influence factors on $\Delta^{14}CO_2$, include interhemispheric transport, ocean circulation, nuclear power plants and terrestrial biosphere, will be discussed later.

In this review, we focus on the newly added $FFCO_2$ traced by ^{14}C, mainly present progress in the 21st century. We first present the commonly used method of $\Delta^{14}CO_2$ sampling and measuring, as well as the basic theory of $FFCO_2$ calculation (Section 2). Then, we summarize the atmospheric $\Delta^{14}CO_2$ trend in several representative background sites, which is essential to the calculation of $FFCO_2$ (Section 3). In Section 4, we reviewed the measurements of $\Delta^{14}CO_2$ and the calculated $FFCO_2$ concentrations globally and present the spatial patterns and temporal variations. The recent progress of the combination of ^{14}C measurements and atmospheric transport models to interpret $FFCO_2$ concentration and its cross-regional transport, and to estimate the emissions of $FFCO_2$, are also reviewed.

2. The Basis of Tracing Fossil Fuel CO_2 Using ^{14}C

2.1. The Theory of Quantifying Fossil Fuel CO_2 Using ^{14}C

Observed CO_2 mole fraction (or concentration) is thought to be a mixing of many components, mainly including atmospheric background CO_2, fossil fuel CO_2, biospheric CO_2 and oceanic CO_2. The most commonly used method to constrain recently added $FFCO_2$ in the atmosphere with ^{14}C is called the pseudo-Lagrangian method [25–27], in which a parcel of air with an initial CO_2 mixing ratio (CO_{2bg}) and $\Delta^{14}CO_2$ value (Δ_{bg}) moves across a polluted region, and then CO_2 mixing ratio and $\Delta^{14}CO_2$ value are modified to CO_{2obs} and Δ_{obs} by the addition of $FFCO_2$ and other sources or sinks of CO_2. If combining other sources (and sinks) together, the mixing ratio and the $\Delta^{14}CO_2$ value could be written as CO_{2other} and Δ_{other}. Two balance equations for CO_2 mixing ratio and $\Delta^{14}C$ can be formulated as below.

$$CO_{2obs} = CO_{2bg} + CO_{2ff} + CO_{2other} \quad (2)$$

$$\Delta_{obs}CO_{2obs} = \Delta_{bg}CO_{2bg} + \Delta_{ff}CO_{2ff} + \Delta_{other}CO_{2other} \quad (3)$$

By combining Equations (2) and (3), CO_{2ff} can be calculated as:

$$CO_{2ff} = \frac{CO_{2obs}\left(\Delta_{obs} - \Delta_{bg}\right)}{\Delta_{ff} - \Delta_{bg}} - \frac{CO_{2other}\left(\Delta_{other} - \Delta_{bg}\right)}{\Delta_{ff} - \Delta_{bg}}. \quad (4)$$

CO_{2obs}, Δ_{obs} are measured in collected samples at interested sites. Δ_{bg} is measured in samples from background sites in general, while free tropospheric measurements can also act as Δ_{bg}, too [13]. Δ_{ff} is known to be $-1000‰$ since CO_{2ff} is ^{14}C-free.

The second term of Equation (4) is bias due to the effect of the others:

$$\beta = \frac{CO_{2other}\left(\Delta_{other} - \Delta_{bg}\right)}{\Delta_{ff} - \Delta_{bg}}. \quad (5)$$

some researchers assume β to be zero, which means that all other sources have the same $\Delta^{14}C$ compared to those of the background atmosphere, $\Delta_{other} = \Delta_{bg}$ [26]. The main contributor to uncertainties in β would be heterotrophic respiration, which has large ^{14}C disequilibrium. The ignorance of β would cause a systematic underestimation of CO_{2ff}, up to 0.5 ppm in summer and 0.2 ppm in winter [13,27]. There are two other factors that influence atmospheric $\Delta^{14}CO_2$, air-sea exchange in the oceans, and stratosphere-troposphere transport [28]. However, these exchanges are assumed to affect the background and observed samples equally; thus, normally, they will not be counted in the calculation of $FFCO_2$.

2.2. Air Sampling and Measurement

Atmospheric $\Delta^{14}CO_2$ can be measured with direct air sampling. Whole air samples are normally collected using flasks or bags. Short-period and integrated samples can be collected by pump and acid solution, respectively. CO_2 samples can be collected by static absorption using CO_2-free sodium hydroxide (NaOH) or barium hydroxide (BaOH) solutions in flasks [25,29,30]. The primary collection method is the static absorption of CO_2 using CO_2-free sodium hydroxide (NaOH) or barium hydroxide (BaOH) solutions in discrete glass flasks [25,29]. The flasks are exposed to air for collection of integrated samples. Besides ground sites, tall towers, aircrafts, balloons, and even kites are all effective platforms to collect CO_2 samples [13,31–34].

Air samples reflect near real-time atmospheric $\Delta^{14}CO_2$, can be used to characterize the $FFCO_2$ temporal variations with high resolution effectively. However, the representativeness of the air samples is limited to those of the sampling region and period, while little information (spatial and temporal distribution) is known beyond that. In addition, the sample collecting process and/or the site maintenance is labor and cost intensive. Direct sampling of air is not the only way to analyze atmospheric $\Delta^{14}CO_2$. Plants fix CO_2 from the atmosphere via photosynthesis, offering a unique complementary analysis method.

For plants, their carbon isotopic composition can be used to reflect the mean atmosphere $\Delta^{14}CO_2$ isotopic composition of their growing period. By collecting plant samples in different regions and analyzing ^{14}C, $FFCO_2$ spatial distribution on a large scale can be mapped out. Compared to air samples, collecting plant materials is more convenient and relatively cheap. Tree rings and annual leaves (grasses) are two main types used to reveal the spatiotemporal distribution of $FFCO_2$ [30,35–40]. Each plant species may have its own advantages in addition to those illustrated above. Maize is grown in many countries, so it is convenient to map out the large-scale spatial distribution of fossil fuel influences using corn leaves. Gingko is a perennial and deciduous tree that is widely planted in East Asian countries, urban areas, and rural areas. Thus, it is feasible to separate samples of clean sites from samples of polluted sites. Wine ethanol is a unique plant material that can represent previous sampling years, since the harvest year and region are all written on the label of the wine bottle. Tree rings, a unique plant material, help in the reconstruction of annual atmospheric $\Delta^{14}CO_2$ for decades or hundreds of years. In practice, however, the sampling

of tree rings may be more difficult than that of annual plants since it is difficult to separate one annual ring from the others.

Comparisons of $\Delta^{14}CO_2$ and/or $FFCO_2$ between plant materials and air samples show nearly consistent results [30,41–43], which verifies the usage of plant materials. Xiong et al. [44] found a significant difference in $\Delta^{14}CO_2$ between respired CO_2 and bulk organic matter from 21 plant species, suggesting that bias associated with dark respiration should be considered when use ^{14}C in plants to quantify atmospheric $FFCO_2$. It should be noted that biomass accumulated by plants only represents daytime $\Delta^{14}CO_2$ (when photosynthesis occurs), and the sampling should be well planned for different plant species considering their growing period and local climate.

Before the analysis of ^{14}C, the preparations of air samples included extracting the CO_2 (purification), and the reduction of CO_2 to graphite. The extraction of CO_2 is to remove water cryogenically, freeze CO_2 completely together with N_2O (non-interfering), and without freeze O_2 or CH_4 [13,45]. Graphite is produced by adding hydrogen gas to CO_2 over an iron catalyst [46,47]. The atom counting of each graphite sample is then performed by an accelerator mass spectrometer (AMS). The preparation of annual leaves is a little different from air samples: plant samples need to (1) be cleaned by pure water and then dried, (2) be combusted to CO_2 and then reduced to graphite [35].

Direct atom-counting of ^{14}C using AMS is a great progress of ^{14}C analysis methods. Before that, the conventional methods were decay counting, solid carbon using a Geiger–Muller counter, and liquid scintillation counting [48]. The sensitivity was improved around 10^6 times by AMS over the decay counting methods [49]. With the attempts to reduce sample size and to increase precision, the detection limits have been reduced to ~5 μg of carbon [50,51], and the reported precisions have reached 1‰ [17].

3. Atmospheric $\Delta^{14}CO_2$ Trend in Background Sites

To characterize the newly added atmospheric $FFCO_2$, it is necessary to first study the $\Delta^{14}CO_2$ variations at background sites. Background sites are located in remote areas (high mountain, coastal area, etc.), rarely influenced by local pollution. When analyzing $\Delta^{14}CO_2$ values from certain sites to deduce the contribution of local or regional fossil fuels, $\Delta^{14}CO_2$ measured at background sites helps separate it from continental trends. In this study, we summarize the background $\Delta^{14}CO_2$ measurements in the last two decades from six representative background sites, including Jungfraujoch and Schauinsland (Europe), Niwot Ridge and La Jolla (North America), Waliguan (Asia), and Wellington (Oceania) (Figure 1).

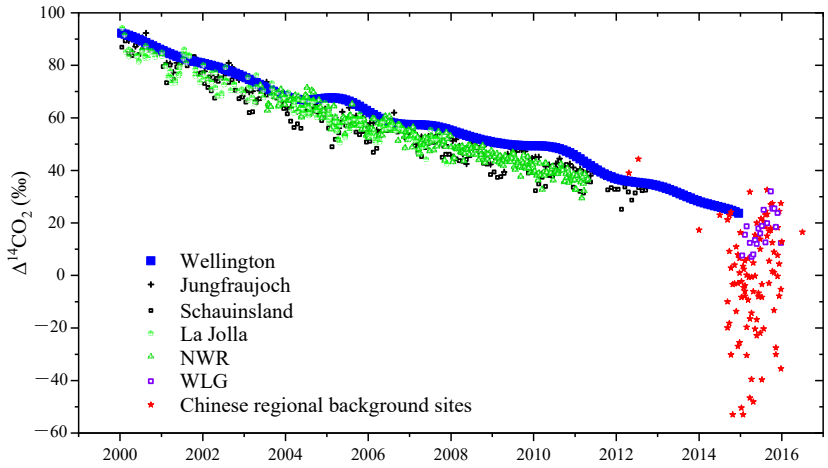

Figure 1. $\Delta^{14}CO_2$ measurements of background sites. Blue square: Wellington, Newzealand [52]; black cross: Jungfraujoch, black box: Schauinsland, Europe [53]; semi-filled green circle: La Jolla, green triangle: Niwot Ridge, North America [54–56]; purple box: Waliguan, China [57,58]; other red symbols: regional background sites in China, Shangdianzi, Luhuitou, Li'an, Longfengshan [57].

In Europe, Jungfraujoch (JFJ) and Schauinsland (SIL) are the two most representative background sites. Jungfraujoch is located in the Swiss Alps at an elevation of 3450 m a.s.l. and mostly samples air from the free troposphere over [59]. Schauinsland is in Black Forest, Germany, with an elevation of 1205 m a.s.l. Schauinsland normally samples free tropospheric air during the night but is influenced by boundary layer air during the day [60]. The two stations all use 2-week integrated CO_2 samples collected by NaOH solution absorption. Levin et al. [53] found $\Delta^{14}CO_2$ in both sites showed a steady decreasing trend, about 6‰ per year at the beginning of the 21st century and 3‰ per year on average in 2009–2012. The seasonal features of $\Delta^{14}CO_2$, they are similar for nearly all the background sites, with maxima recorded during summer/autumn and minima during winter/spring.

Niwot Ridge (NWR), Colorado, USA, has a high elevation (3475 m a.s.l.) continental site, can be used as a proxy for North American free tropospheric air [56]. The measurement of $\Delta^{14}CO_2$ began in 2003 using whole air samples. According to Turnbull et al. [56], $\Delta^{14}CO_2$ at NWR decreased by 5.7‰ per year from 2004 to 2006, with a seasonal amplitude of 3–5‰. Lehman et al. [55] extend the dataset to 2011. Measurement in La Jolla, California, is conducted at the Scripps Pier, using whole air samples when meteorological conditions are favorable for collecting clean marine air [54]. The monthly samples show a decreasing trend of 5 ± 0.2‰ per year from 2001 to 2007. The decreasing trends in North American background sites are similar to the two European stations. NWR appears to be a reasonable choice of background air for Northern Hemisphere midlatitude and has been used as background CO_2 and $\Delta^{14}CO_2$ to quantify $FFCO_2$ [27,58].

Compared to Europe and North America, the measurements of $\Delta^{14}CO_2$ in Asian sites are not continuous. Waliguan (WLG) Global Atmosphere Watch (GAW) station, located on top of Mt. Waliguan (3816 m a.s.l.), the northeast part of the Qinghai-Tibetan Plateau, represents the background air for the Eurasian continent. Since $\Delta^{14}CO_2$ is not measured conventionally on this site, there is only a small amount of data [57,58]. $\Delta^{14}CO_2$ values at WLG during 2004/2005 are close to those measured at NWR [58]. Even though the values of WLG in 2015 are lower than the other background sites in previous years, they may be similar considering the annual trend at other sites. The observations at some regional background sites in China are also shown in Figure 1, all collected during a short period and mostly lower than the values in the WLG [9].

The world's longest direct record of atmospheric $\Delta^{14}CO_2$ was begun at Wellington, New Zealand, in 1954 [52,61]. The sampling sites in Wellington are located in the coastal areas of two islands. Through decades of measurement, the collection method and measurement method have changed several times (details in [52]). In the 21st century, $\Delta^{14}CO_2$ in Wellington is consistently higher than in Northern Hemispheric sites, as shown in Figure 1. Based on seven global stations, Graven et al. [28] found that the mean $\Delta^{14}CO_2$ in the Northern Hemisphere was 5‰ lower than that in the Southern Hemisphere over 2005–2007. The interhemispheric exchange time is estimated to be 1.4 years [56,62]. Many researchers have interpreted these contributions to the interhemispheric gradient [24,28,52]. The major cause includes the dilution by ^{14}C-free fossil fuel emissions in the north, and the weakening of ^{14}C-depleted ocean upwelling in the south. The oceans are the largest reservoir of carbon, and the principal natural drivers that are responsible for atmospheric $\Delta^{14}CO_2$. Air-sea ^{14}C flux is greatly influenced by ocean circulation and atmosphere-ocean CO_2 exchange. The reducing ^{14}C uptake and the weakening ^{14}C-depleted upwelling in the Southern Ocean resulted in a decrease in atmospheric $\Delta^{14}CO_2$ [24].

Among all background sites, the annual decreasing trends of $\Delta^{14}CO_2$ in the 21st century are similar. According to the observations and modeling conducted by Levin et al. [24], the global long-term trend in $\Delta^{14}CO_2$ is main influenced by fossil fuel emissions since the 1990s. If fossil fuel emissions continue to increase in a "business-as-usual" scenario in the IPCC Fifth Assessment Report, $\Delta^{14}CO_2$ will likely drop below the preindustrial level (0‰) in a decade and be reduced to −250‰ by the year 2100. However, if ambitious emission reductions could be conducted, $\Delta^{14}CO_2$ will be sustained near the preindustrial level through 2100 [63].

In general, it is recommended that the quantification of $FFCO_2$ need to refer to the corresponding background $\Delta^{14}CO_2$ values and CO_2 concentrations, due to the spatial gradients in $\Delta^{14}CO_2$. However, Turnbull et al. [58] estimated $FFCO_2$ in South Korea with four different background sites (WLG, NWR, Mauna Loa, Hawaii, and Ulaan Uul, Mongolia) separately, and found no substantial change in the results. The enhancements above baseline are typically large compared to the differences caused by the choice of background.

4. Spatial and Temporal Variations of $\Delta^{14}CO_2$ and $FFCO_2$

To provide a periodical review of the spatiotemporal characteristics of $FFCO_2$, we collected $\Delta^{14}CO_2$ measurements of air and plant samples and/or the calculated $FFCO_2$ reported in the past two decades (Table 1). Since measurements in Europe and North America have been implemented for decades, we focus more on the recent measurements in Asia (Figure 2, where CO_2 emissions are higher than in other regions [64]). The global $FFCO_2$ distribution is plotted in Figure 3.

Table 1. $\Delta^{14}CO_2$ measurements and calculated $FFCO_2$ concentrations reported in the last two decades.

Location	Sampling Period		$^{14}CO_2$ (‰)	$FFCO_2$ (ppm by Defult)	Site Type/Name	Note (Air Samples with No Notes)	References
Hungary	September 2008–April 2009		−4.5~39.1		city		[65,66]
			23.1~48.1		rural (10 m)		
			31.4~47.3		rural (115 m)		
Netherlands	2010–2012		35.2, 27.2, 22.6			corn leaves	[42]
Germany	2012		17.2				
France	2012		31.7				
Poland	July 2011–May 2013		−178.2~4.7	66.6~72.7%			[43]
Romania	August 2012–January 2018		–57~61		industrial area		[67]
Switzerland	June 2013–December 2015			4.3	tall tower		[7]
England	June 2014–August 2015		−35.26~59.61	−1.09~2.27	tall tower		[68]
North America	2004, summer		66.3 ± 1.7		mountain regions, western North America	corn leaves	[35]
			58.5 ± 3.9	2.7 ± 1.5	eastern North America		
			55.2 ± 2.3	4.3 ± 1.0	Ohio-Maryland region		
California, USA	2004–2005		59.5 ± 2.5	0.3 ± 0.08	North Coast	annual C3 grasses	[37]
			44 ± 10.9	6.1 ± 1.1	San Francisco		
			48.7 ± 1.9	4.8 ± 0.9	Central Valley		
			27.7 ± 20	13.7 ± 0.4	Los Angeles		
Los Angeles, USA	2006–2013		−59.4~29.3		inland Pasadena		[69]
	2009–2013		−18.8~40.4		coastal Palos Verdes		
high latitudes,	2008	spring	46.6 ± 4.4			flight	[70]
North America		summer	51.5 ± 5				
central California, USA	2009–2012	winter		7.2	Walnut Grove		[71]
		spring		3.1			
		summer		3.7			
		fall		5.0			

Table 1. *Cont.*

Location	Sampling Period		$^{14}CO_2$ (‰)	$FFCO_2$ (ppm by Defult)	Site Type/Name	Note (Air Samples with No Notes)	References
southern California, USA	2013–2014	winter		25	California Institute of Technology in Pasadena		
		spring		21.6			
		summer		25.9			
		fall		21.5			
		winter		8.2	San Bernardino		
		spring		5.1			
		summer		11			
		fall		10.2			
Mexico City	March 2006		20~132				[72]
South Korea	2009		−112.3~−12.4	4.2~13.9	Seoul, metropolitan area	gingko leaves	[73]
			−79.5~43.8	−1.3~10.7	Busan, metropolitan area		
			–69.3~28.1	0.2~9.7	Daegu, metropolitan area		
			−53.4~−2	3.2~8.2	Daejeon, metropolitan area		
			−41.7~19.2	1.1~7	Gwangju, metropolitan area		
South Korea	2009		34.8		clean air sites	gingko leaves	[38]
	2010		24.9				
	2011		23.1				
	2012		14				
	2013		8.3				
Anmyeondo, South Korea	May 2014–August 2016		−59.5~23.1	9.7 ± 7.8			[9]
Tae-Ahn Peninsula,	2004–2010	all year		4.4, 60%			[58]
South Korea		winter		4.4, 90%			
Beijing	March 2009–September 2009		3.4 ± 11.8	16.4 ± 4.9			[74]
			12.8 ± 3.1		suburban sites		
			−8.4 ± 18.1		road sites		
	2009		−28.2~29.6			corn leaves	[75]
	2014		−53.5 ± 54.8	39.7 ± 36.1, 75.2 ± 14.6%	urban site		[76]
Guangzhou	2010–2011		–16.4 ± 3.0	24 (1–58)			[77]
Xiamen	2014		−8.7 ± 25.3	13.6 ± 12.3, 59.1 ± 26.8%	urban site		[76]
Xi'an	March 2012–March 2013		−41.3 ± 27.4				[30]
	April 2012		−9.7 ± 23.8				
	January 2013		−90.4 ± 32.4				
	March 2012.03–March 2013			34.2 ± 9.5			
	March 2012–March 2013	winter		46.5 ± 8.7			
	March 2012–March 2013	summer		26.6 ± 3.4			
Xi'an	2013	summer		20.5		annual plants	[78]
	2014	summer		23.5			
Xi'an	2014	winter		92.7 ± 9.7			[79]
	2016	winter		61.8 ± 10.6	urban		[80]
	2016	winter		57.4 ± 9.7	suburban		
	2016	summer		82.5 ± 23.8	urban		
	2016	summer		90 ± 24.8	suburban		
Bali, Indonesia	September 2018		2.2 ± 19	6.4 ± 7.5		evergreen leaves	[81]

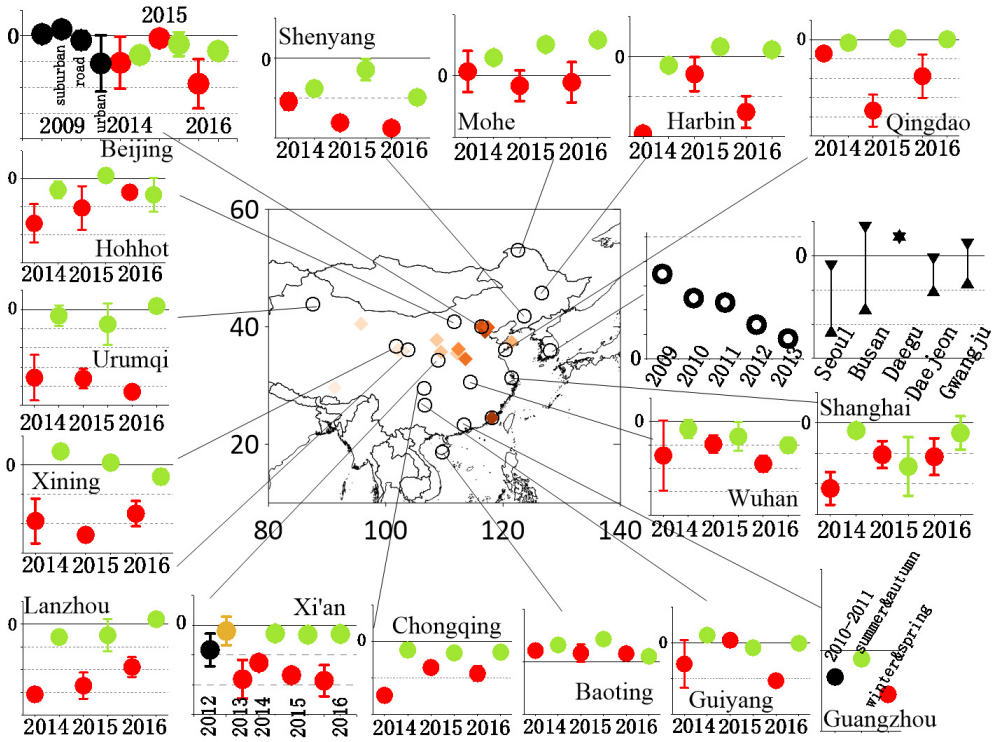

Figure 2. The spatial distribution of $\Delta^{14}CO_2$ in Asia. Orange diamonds in the map denote the sites with $\Delta^{14}CO_2$ values [9,30,38,57,73–75,77–80,82]. The scatter plots outside the map denote the time serials of $\Delta^{14}CO_2$ measurements, the main grid line (solid) represents the $\Delta^{14}CO_2$ value is zero, and the $\Delta^{14}CO_2$ value between every two dashed lines represents a difference of 50‰. Green dots: summer months, red dots: winter months, black symbols: yearly values, brown dot: autumn months.

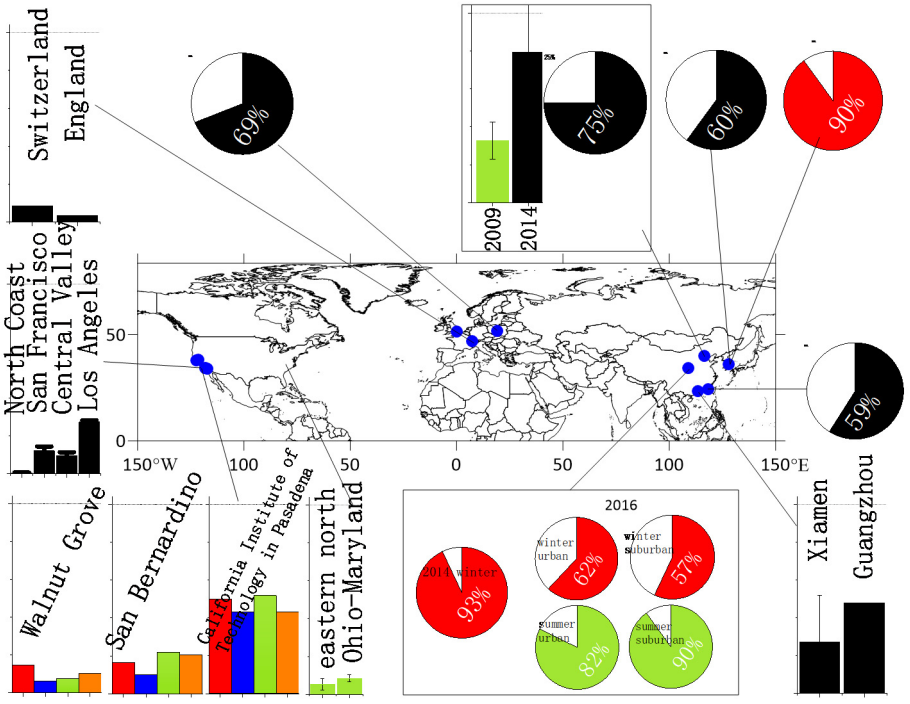

Figure 3. The spatial distribution of $\Delta^{14}CO_2$ traced $FFCO_2$. The percentage in pie charts represents the fossil fuel component to total CO_2. The grid lines in histograms represent that the $FFCO_2$ value is 50 ppm. Colors in pie charts and histograms: blue-spring, green-summer, orange-autumn, red-winter, black- yearly values [7,9,35,37,43,58,71,74,76,77,79,80,83].

4.1. Spatial Patterns of $\Delta^{14}CO_2$ and $FFCO_2$

$\Delta^{14}CO_2$ measurements in Asia are mostly carried out in China, South Korea, and Japan around the 2010s. There are great differences in $\Delta^{14}CO_2$ values among cities. Highest $\Delta^{14}CO_2$ values appear in cities in middle and western China (light orange diamonds in Figure 2), where are sparsely populated. The $\Delta^{14}CO_2$ values measured in Northeast China (Mohe, Harbin, and Shenyang) and in coastal areas (Baoting, Xiamen, and Guangzhou) are also higher than those in other cities. Lower $\Delta^{14}CO_2$ values are observed in the winter months in western China (Urumqi, Xining, and Lanzhou) and in big cities in eastern China (Qingdao, Shanghai, and Beijing). For South Korea, the annual averaged $\Delta^{14}CO_2$ values from the clean sites (Gingko leaves) are consistently above zero, but the values in metropolitan areas are much lower [38,73,82]. Plant materials only represent $\Delta^{14}CO_2$ in the growing period, which is normally from late spring to early autumn in Asia. Similar spatial patterns of measured $\Delta^{14}CO_2$ are found in Beijing and Xi'an. In Beijing, $\Delta^{14}CO_2$ values at urban sites are significantly lower than those observed at suburban sites, and road sites are mostly lower than park sites and campus sites [74,76]. For the observations in Xi'an, $\Delta^{14}CO_2$ values at suburban sites are significantly and consistently higher than those for urban sites in both winter and summer [80]. On a larger scale, the $\Delta^{14}CO_2$ values inside the Guanzhong basin, where the capital city Xi'an is located, are lower than the edge and outside the basin [84,85]. The influence of topography also appears in Beijing, where the $\Delta^{14}CO_2$ values in the northwest area (mountain area) are lower than those in the southeast area due to different dispersion situation [74].

$FFCO_2$ concentrations calculated with $\Delta^{14}CO_2$ measurements were carried out in fewer cities. Corresponds to the spatial patterns of $\Delta^{14}CO_2$, $FFCO_2$ concentrations are higher in Beijing (39.7 ppm in 2014) and Xi'an (34.2 ppm, 2012–2013), and lower in Xiamen (13.6 ppm, 2014) and Guangzhou (24 ppm, 2010–2011) [30,76,77]. In Bali, Indonesia, $FFCO_2$ concentrations in densely populated areas reach 25 ppm, while they are lower than 1 ppm in cleaner sites ($\Delta^{14}CO_2$ varies from −46‰ to 18‰ [81]). For regional background sites, $FFCO_2$ concentrations are 12.7 ± 9.6 ppm in Lin'an, 11.5 ± 8.2 ppm in Shangdianzi, 4.6 ± 4.3 ppm in Luhuitou (2014–2015 [57]), and 9.7 ± 7.8 ppm in Anmyeondo (2014–2016 [9]). This means that using a regional background site to quantify $FFCO_2$ would cause a certain underestimation. Most of these studies provided the spatial characteristics of $FFCO_2$ in these cities for the first time, reflecting current emissions and offering a basis for emission reduction.

In North America, based on samples of corn leaves collected during the summer of 2004, mountain regions of western North America show the smallest influence of $FFCO_2$ with a mean $\Delta^{14}CO_2$ of 66.3 ± 1.7‰, while Eastern North America and the Ohio-Maryland region show a larger fossil fuel influence with a mean $\Delta^{14}CO_2$ of 58.8 ± 3.9‰ and 55.2 ± 2.3‰, respectively [35]. California is another hotspot influenced by fossil fuel, with mean $\Delta^{14}CO_2$ values of 44.0 ±10.9‰ in San Francisco, and 27.7 ± 20.0‰ in Los Angeles (winter annual grasses [37]). Large regional gradients were captured near urban areas. Take the Los Angeles megacity as an example, $\Delta^{14}CO_2$ in inland Pasadena (2006–2013) and coastal Palos Verdes peninsula (2009–2013) are about −14.2‰ and 15.0‰, respectively [69]. It seems that $\Delta^{14}CO_2$ values are higher in North America than in Asia, based on the above-mentioned studies. The reason may be that the measurements in Asian cities were mostly implemented in the 2010s, about 5 to 10 years later than those in North America. Considering that the decreasing trend of $\Delta^{14}CO_2$ in background sites is about 5‰ per year, there are no significant differences in $\Delta^{14}CO_2$ values of cities between those two areas. For the newly added $FFCO_2$ calculated with $\Delta^{14}CO_2$, the values were over 20 ppm in southern California (2013–2014 [71]), while those in the other parts in North America are consistently lower than 10 ppm, e.g., 2.9–8 ppm in central California, 2.7 ppm and 4.3 ppm in eastern North America and Ohio-Maryland region (2004 summer [35]).

As for Europe, $\Delta^{14}CO_2$ has been analyzed in countries including Hungary [65,66], Netherlands, Germany, France [42], Switzerland [7], Romania [67], England [68], Poland [43], etc. Plant samples collected from 51 different locations in the Netherlands, Germany, and France, together with model outputs, all capture the regional $\Delta^{14}CO_2$ gradients.

Bozhinova et al. [42] presume that the largest gradients found in the Netherlands and Germany are associated with emissions from energy production and road traffic. In France, the $\Delta^{14}CO_2$ enrichment from nuclear sources dominates in many samples. Similar regional gradients are also found in Poland between the built-up area of the city and several kilometers from the city center [43]. For $FFCO_2$, long-term mean (1986–2002) concentration in Heidelberg, Germany is about 10.5 ppm [26]. In Hungary, the winter peaks were about 10–15 ppm, similar to those in Germany, although they were measured during 2008–2010 [65,66]. The concentrations of $FFCO_2$ calculated using tower-based samples are much lower. In Switzerland, the averaged concentration of $FFCO_2$ sampled at a 212.5 m tower is 4.3 ppm (2013–2015 [7]). In the UK, the concentration is 1.8 ppm (2014–2015) from a 185 m tower [68]. In the high latitude areas of Eurasia, train-based $\Delta^{14}CO_2$ observations from Western Russia to Eastern Siberia show an increase in $\Delta^{14}CO_2$, which shows large $FFCO_2$ emissions in heavily populated Europe, and gradual dispersion of the fossil fuel plume across Northern Asia [86].

4.2. Temporal Variations of $\Delta^{14}CO_2$ and $FFCO_2$

Most cities in the North Hemisphere show significant seasonal differences with $\Delta^{14}CO_2$ values higher in summer and lower in winter, including Jungfraujoch, Schauinsland [53], Heidelberg [87], Krakow (Poland [43]), Guangzhou [77], Beijing [88], Xi'an [30,79,80,89] and cities in Figure 2 sourced from Zhou et al. [79]. Consequently, $FFCO_2$ concentrations calculated with $\Delta^{14}CO_2$ in winter are higher than in summer [30,77,88,90]. For example, the $FFCO_2$ concentration is 14 ppm in winter and 6.5 ppm in summer Heidelberg [26]. This may be interpreted by the increased fossil fuel consumption and lower boundary layer height in winter, and the intensive biogenic photosynthesis in summer. However, seasonal variations of $\Delta^{14}CO_2$ (and/or $FFCO_2$) in some cities are not significant, e.g., in Baoting and Xiamen, China [79,88]. These cities are relatively warm in winter, so there is less fossil fuel consumption for heating. For Gliwice, Poland, Piotrowska et al. [43] attributed this to fluctuations in the measurements resulting from the methodology.

Diurnal variations of $FFCO_2$ (and/or $\Delta^{14}CO_2$) are examined with measurements at high temporal resolution. High concentrations of $FFCO_2$ commonly occur during morning and afternoon rush hours, which obviously result from transportation emissions (Germany [14]; China [76]). Some cities observed nighttime $FFCO_2$ peaks, which could be related to weak nocturnal atmospheric dispersion, especially the relatively low planetary boundary layer [76,84]. Diurnal $FFCO_2$ also showed evident variations in the background areas. Niu et al. [88] found that the $FFCO_2$ concentrations at SDZ decreased rapidly from 31.6 ± 1.3 ppm at 00:00 to 0 ppm at 04:00 during the winter sampling days.

5. Estimation of $FFCO_2$ and Its Emissions Combining Numerical Models

How to interpret the measurements is also of vital importance, especially with relatively sparse datasets. Here, we present the studies combining $\Delta^{14}CO_2$ measurements (and/or the calculated $FFCO_2$) and atmospheric transport models to provide insights into the variation of atmospheric $FFCO_2$ concentration, to quantify the cross-regional transport, and to estimate the emissions of $FFCO_2$, etc. Hsueh et al. [35] collected samples from 67 sites across North America and estimated the spatial distribution of carbon sources and sinks with the help of transport models, and further identified fossil fuel emissions as the major driver of regional variability. Riley et al. [37] used a regional transport model to simulate anthropogenic and ecosystem CO_2 fluxes in California. The model well reproduced the regional patterns of $FFCO_2$, and quantified its fluxes in different directions. Moreover, the model simulations indicated that some areas with high near-surface $FFCO_2$ mixing ratios may not be expected from local emissions inventories. Wenger et al. [68] developed isotope modeling to simulate $^{12}CO_2$, $^{13}CO_2$, and $^{14}CO_2$ directly, and by which they calculated the impact of nuclear and biospheric disequilibrium.

When discussing the observation–model comparisons, possible systematic model biases and short-term observation anomalies need to be noticed. Lafranchi et al. [31] found

that their $\Delta^{14}CO_2$ observations cannot be reproduced by model simulations, with the terrestrial biosphere being responsible for a significant contribution. The interpretations of observation–model comparisons can also be different between air and plant samples, since the latter offers integrated daytime $\Delta^{14}CO_2$ over months. Influenced by local weather information, plant species, etc., the accumulation of CO_2 may vary during different growing periods. To address this problem, Bozhinova et al. [91] use a crop growth model to reproduce daily fixation of $\Delta^{14}CO_2$ in maize and wheat plants by making a weighted average of the daily contribution from the atmospheric $\Delta^{14}CO_2$ mixing ratios. The simulations suggest that the influence of day-to-day plant growth on recorded $\Delta^{14}CO_2$ signals is not negligible when interpreting plant sampled $\Delta^{14}CO_2$ values [41,42].

The measurements of $\Delta^{14}CO_2$ and the derived $FFCO_2$, combined with transport models, offer an appealing method for evaluating and optimizing the emissions of $FFCO_2$ (inverse method). Traditionally, $FFCO_2$ emission inventories are derived from energy and fuel use statistics, combustion efficiencies, and emission factors ("bottom-up" method). These are the basic knowledge for $FFCO_2$ emissions, but the uncertainties for national annual inventories in developed countries may be 5–10% and even larger in developing countries or on smaller scales with finer resolution [92,93]. For example, the relative differences of $FFCO_2$ emissions of China based on nine emission inventories are approximately 21%. The provincial-level spatial distribution shows more consistency, while the top 5% of the grid level accounts for 50–90% of total emissions [94]. Inverse modeling is a statistical method used to estimate emissions by narrowing the mismatch between simulations and observations. It has long been used to constrain emissions of CO_2 [95,96], other greenhouse gases, CO, black carbon, [97,98] etc. The big advantage of inverse methods is that the evaluation is more accurate and independent. Turnbull et al. [58] compared modeled and observed $FFCO_2$ (derived from $\Delta^{14}CO_2$), and the results are consistent with each other when considering a 63% increase in emissions. Turnbull et al. [99] evaluated $FFCO_2$ emissions of a point source, the uncertainties of which were better than 10%, representing an improvement by a factor of 2. According to Basu et al. [100], the uncertainties of $FFCO_2$ emissions for the US national can be constrained within 1% for a whole year and within 5% for most months. Thus, this method may act as an independent way to assess emission reductions and regulations under a global warming background. It should be noted that there are internal errors in the inverse methods, including representation errors, aggregation errors, systematic errors in the transport model, etc. [101]. Thus, the propagation of errors between the $\Delta^{14}CO_2$ measurements and the inverse models needs to be carefully considered. Moreover, three or more sites are required for the further reduction of uncertainty in the estimates of $FFCO_2$ emissions [102].

6. Conclusions and Outlook

Radiocarbon (^{14}C) is a reliable and promising tool for quantifying fossil fuel components in atmospheric CO_2 ($FFCO_2$). Focusing on the quantification of the atmospheric concentrations and emissions of $FFCO_2$, we reviewed the $^{14}CO_2$ measurements and the calculated $FFCO_2$ concentrations conducted mainly in the last two decades. Spatial-temporal characteristics were presented, and the recent progress of the combination of ^{14}C measurements and atmospheric transport models was also discussed. As the most accurate method to quantify $FFCO_2$, the radiocarbon technique is promising, although there are several issues that need to be improved currently. Nuclear power plants play a significant role in the quantification of $FFCO_2$, since the enrichment by $\Delta^{14}CO_2$ from nuclear sources can partly mask, or even exceed the influence from fossil fuel emissions in some regions [41,68,103]. Thus, $\Delta^{14}CO_2$ values need to be corrected before quantifying $FFCO_2$. The combination of atmospheric transport models and reported nuclear industry emissions offers a solution to this issue [104,105]. As for the $FFCO_2$ emission estimation, it is complex for urban areas, where most $FFCO_2$ emit from. With the coexistence of biomass burning and/or heterotrophic respiration, the emissions of $FFCO_2$ may be underestimated. As

illustrated in Section 2.1, the "other" term needs to be carefully considered regarding the sources and sinks in the catchment area.

Based on different projections of future CO_2 emissions and atmospheric concentrations, new issues related to ^{14}C techniques will emerge. The sensitivity of $\Delta^{14}CO_2$ to newly added $FFCO_2$ diminishes with an increase in atmospheric $FFCO_2$. For example, the atmospheric CO_2 concentration and ^{14}C value were ~380 ppm and 66‰, respectively, in 2003. Thus, 1 ppm of ^{14}C-free $FFCO_2$ added to the atmosphere will produce a $^{14}CO_2$ depletion of ~2.8‰ [13]. For the year 2015, atmospheric CO_2 concentration and ^{14}C value were ~400 ppm and 17‰ (WLG), respectively, resulting in a depleting rate of ~2.5‰ ppm^{-1}-CO_2. This trend is likely to continue in the near future if the emissions of greenhouse gases follow the high, very high, and intermediate scenarios as IPCC assessed. This requires a more precise measurement of ^{14}C to maintain the current detection capabilities. Meanwhile, the deep ocean upwelling in the Southern Hemisphere may provide ^{14}C-enriched CO_2 rather than ^{14}C-depleted CO_2 comparing to atmospheric $\Delta^{14}CO_2$. On the contrary, if CO_2 removal and emission reduction can be effectively conducted, the ocean and terrestrial ecosystem will shift from carbon sinks to carbon sources as net CO_2 emissions become negative. Under either circumstance, $\Delta^{14}CO_2$ fluxes and their influences on $FFCO_2$ quantification need to be reconsidered.

Because the importance of CO_2 emission control has attracted worldwide attention, future fossil fuel fractions in total CO_2 may be greatly influenced by policy factors. According to the Climate Ambition Alliance: Net Zero 2050, more than 100 nations have committed to getting carbon neutral (also called net zero), which means that the CO_2 released into the atmosphere is balanced by its removal from the atmosphere. The CO_2 emissions of these countries account for over 65% of the global total emissions. For example, China announced a carbon peak by 2030 and carbon neutrality by 2060 at the Group of 20 (G20) summit in 2020. According to the guideline to reach carbon peak by 2030 (http://www.gov.cn/zhengce/content/2021-10/26/content_5644984.htm, released in October 2021, latest access on 1 November 2021), the main goals include adjusting the industrial and energy structures, and raising the share of non-fossil fuel energy to around 25% by 2030. How to evaluate the effect of these policies scientifically and accurately is of concern. Though "bottom-up" methods may provide CO_2 emissions for each factory and each county, the radiocarbon technique has its irreplaceable advantages: (a) is an independent verification method disturbed by no political willingness, and (b) may quickly respond to rapid CO_2 emission variations. Thus, a comprehensive carbon emission estimation system is highly recommended in the future for the evaluation of $FFCO_2$ emissions, containing a well-designed monitoring network of CO_2 and $\Delta^{14}CO_2$, uniform measurement standard, $FFCO_2$ quantification method, and the corresponding emission inversion modeling. Until now, most of the $\Delta^{14}CO_2$ measurements have been conducted in limited cities, and continuous measurements have been conducted in fewer cities. Thus, the measurements need to be further expanded, especially at background sites. Moreover, stable carbon isotopic compositions (^{13}C) vary with different types of fossil fuels (coal and liquid fossil fuels) and industrial processes [106], and can also provide more information on the ecosystem carbon cycle. Therefore, the combination of ^{14}C and ^{13}C may further help refine the partitioning of source apportionments for atmospheric CO_2.

Author Contributions: Conceptualization, Y.-L.Z. and M.-Y.Y.; writing—original draft preparation, M.-Y.Y.; writing—review and editing, M.-Y.Y., Y.-C.L. and Y.-L.Z. All authors have read and agreed to the published version of the manuscript.

Funding: This research was funded by the National Natural Science Foundation of China, grant number 42107123, and the Startup Foundation for Introducing Talent of NUIST, grant number 2021r104.

Institutional Review Board Statement: Not applicable.

Informed Consent Statement: Informed consent was obtained from all subjects involved in the study.

Data Availability Statement: Data available on request.

Conflicts of Interest: The authors declare no conflict of interest.

References

1. IPCC. *Climate Change 2021: The Physical Science Basis*; Cambridge University Press: Cambridge, UK, 2021.
2. Diffenbaugh, N.S.; Singh, D.; Mankin, J.S.; Horton, D.E.; Swain, D.L.; Touma, D.; Charland, A.; Liu, Y.; Haugen, M.; Tsiang, M.; et al. Quantifying the influence of global warming on unprecedented extreme climate events. *Proc. Natl. Acad. Sci. USA* **2017**, *114*, 4881–4886. [CrossRef] [PubMed]
3. Frolicher, T.L.; Fischer, E.M.; Gruber, N. Marine heatwaves under global warming. *Nature* **2018**, *560*, 360–364. [CrossRef] [PubMed]
4. Kraaijenbrink, P.D.A.; Bierkens, M.F.P.; Lutz, A.F.; Immerzeel, W.W. Impact of a global temperature rise of 1.5 degrees Celsius on Asia's glaciers. *Nature* **2017**, *549*, 257–260. [CrossRef] [PubMed]
5. Papalexiou, S.M.; Montanari, A. Global and Regional Increase of Precipitation Extremes under Global Warming. *Water Resour. Res.* **2019**. [CrossRef]
6. Shindell, D.; Smith, C.J. Climate and air-quality benefits of a realistic phase-out of fossil fuels. *Nature* **2019**, *573*, 408–411. [CrossRef]
7. Berhanu, T.A.; Szidat, S.; Brunner, D.; Satar, E.; Schanda, R.; Nyfeler, P.; Battaglia, M.; Steinbacher, M.; Hammer, S.; Leuenberger, M. Estimation of the fossil fuel component in atmospheric CO_2 based on radiocarbon measurements at the Beromünster tall tower, Switzerland. *Atmos. Chem. Phys.* **2017**, *17*, 10753–10766. [CrossRef]
8. Konovalov, I.B.; Berezin, E.V.; Ciais, P.; Broquet, G.; Zhuravlev, R.V.; Janssens-Maenhout, G. Estimation of fossil-fuel CO_2 emissions using satellite measurements of "proxy" species. *Atmos. Chem. Phys.* **2016**, *16*, 13509–13540. [CrossRef]
9. Lee, H.; Dlugokencky, E.J.; Turnbull, J.C.; Lee, S.; Lehman, S.J.; Miller, J.B.; Petron, G.; Lim, J.-S.; Lee, G.-W.; Lee, S.-S.; et al. Observations of atmospheric (CO_2)-C-14 at Anmyeondo GAW station, South Korea: Implications for fossil fuel CO_2 and emission ratios. *Atmos. Chem. Phys.* **2020**, *20*, 12033–12045. [CrossRef]
10. Lopez, M.; Schmidt, M.; Delmotte, M.; Colomb, A.; Gros, V.; Janssen, C.; Lehman, S.J.; Mondelain, D.; Perrussel, O.; Ramonet, M.; et al. CO, NOx and 13CO_2 as tracers for fossil fuel CO_2: Results from a pilot study in Paris during winter 2010. *Atmos. Chem. Phys.* **2013**, *13*, 7343–7358. [CrossRef]
11. Niu, Z.; Zhou, W.; Feng, X.; Feng, T.; Wu, S.; Cheng, P.; Lu, X.; Du, H.; Xiong, X.; Fu, Y. Atmospheric fossil fuel CO_2 traced by (CO_2)-C-14 and air quality index pollutant observations in Beijing and Xiamen, China. *Environ. Sci. Pollut. R* **2018**, *25*, 17109–17117. [CrossRef]
12. Rivier, L.; Ciais, P.; Hauglustaine, D.A.; Bakwin, P.; Bousquet, P.; Peylin, P.; Klonecki, A. Evaluation of SF6, C_2Cl_4, and CO to approximate fossil fuel CO_2 in the Northern Hemisphere using a chemistry transport model. *J. Geophys. Res.* **2006**, 111. [CrossRef]
13. Turnbull, J.C.; Miller, J.B.; Lehman, S.J.; Tans, P.P.; Sparks, R.J.; Southon, J. Comparison of 14CO2, CO, and SF6as tracers for recently added fossil fuel CO2 in the atmosphere and implications for biological CO2 exchange. *Geophys. Res. Lett.* **2006**, *33*. [CrossRef]
14. Vogel, F.; Hamme, S.; Steinhof, A.; Kromer, B.; Levin, I. Implication of weekly and diurnal 14C calibration on hourly estimates of CO-based fossil fuel CO_2 ata moderately polluted site in southwestern Germany. *Tellus B Chem. Phys. Meteorol.* **2010**, *62*, 512–520. [CrossRef]
15. Gamnitzer, U.; Karstens, U.; Kromer, B.; Neubert, R.E.M.; Meijer, H.A.J.; Schroeder, H.; Levin, I. Carbon monoxide: A quantitative tracer for fossil fuel CO_2? *J. Geophys. Res.* **2006**, *111*, D22. [CrossRef]
16. Libby, W.F.; Anderson, E.C.; Arnold, J.R. Age Determination by Radiocarbon Content: World-Wide Assay of Natural Radiocarbon. *Science* **1949**, *109*, 227–228. [CrossRef]
17. Schuur, E.A.G.; Druffel, E.; Trumbore, S.E. *Radiocarbon and Climate Change: Mechanisms, Applications and Laboratory Techniques*; Springer International Publishing: Cham, Switzerland, 2016.
18. Reimer, P.J.; Brown, T.A.; Reimer, R.W. Discussion: Reporting and Calibration of Post-Bomb 14C Data. *Radiocarbon* **2004**, *46*, 1299–1304. [CrossRef]
19. Donahue, D.J.; Linick, T.W.; Jull, A.J.T. Isotope-Ratio and Background Corrections for Accelerator Mass Spectrometry Radiocarbon Measurements. *Radiocarbon* **2016**, *32*, 135–142. [CrossRef]
20. Godwin, H. Half-life of Radiocarbon. *Nature* **1962**, *195*, 984. [CrossRef]
21. Suess, H.E. Radiocarbon Concentration in Modern Wood. *Science* **1955**, *122*, 415–417. [CrossRef]
22. Stuiver, M.; Quay, P.D. Atmospheric14C changes resulting from fossil fuel CO_2 release and cosmic ray flux variability. *Earth Planet Sci. Lett.* **1981**, *53*, 349–362. [CrossRef]
23. Dutta, K. Sun, Ocean, Nuclear Bombs, and Fossil Fuels: Radiocarbon Variations and Implications for High-Resolution Dating. In *Annual Review of Earth and Planetary Sciences*; Jeanloz, R., Freeman, K.H., Eds.; Northwestern Univ, Dept Earth & Planetary Sci: Evanston, IL, USA, 2016; Volume 44, p. 239.
24. Levin, I.; Naegler, T.; Kromer, B.; Diehl, M.; Francey, R.; Gomez-Pelaez, A.; Steele, P.; Wagenbach, D.; Weller, R.; Worthy, D. Observations and modelling of the global distribution and long-term trend of atmospheric 14CO_2. *Tellus B Chem. Phys. Meteorol.* **2010**, *62*, 26–46. [CrossRef]
25. Levin, I.; Schuchard, J.; Kromer, B.; Münnich, K.O. The Continental European Suess Effect. *Radiocarbon* **1989**, *31*, 431–440. [CrossRef]
26. Levin, I.; Kromer, B.; Schmidt, M.; Sartorius, H. A novel approach for independent budgeting of fossil fuel CO2 over Europe by 14CO_2 observations. *Geophys. Res. Lett.* **2003**, *30*. [CrossRef]

27. Turnbull, J.; Rayner, P.; Miller, J.; Naegler, T.; Ciais, P.; Cozic, A. On the use of (CO_2)-C-14 as a tracer for fossil fuel CO_2: Quantifying uncertainties using an atmospheric transport model. *J. Geophys. Res.-Atmos.* **2009**, *114*, D22302. [CrossRef]
28. Graven, H.D.; Guilderson, T.P.; Keeling, R.F. Observations of radiocarbon in CO_2 at seven global sampling sites in the Scripps flask network: Analysis of spatial gradients and seasonal cycles. *J. Geophys. Res.-Atmos.* **2012**, *117*, D02302. [CrossRef]
29. Manning, M.R.; Lowe, D.C.; Melhuish, W.H.; Sparks, R.J.; Gavin, W.; Brenninkmeijer, C.; Mcgill, R.C. The Use of Radiocarbon Measurements in Atmospheric Studies. *Radiocarbon* **1990**, *32*, 37–58. [CrossRef]
30. Zhou, W.; Wu, S.; Huo, W.; Xiong, X.; Cheng, P.; Lu, X.; Niu, Z. Tracing fossil fuel CO_2 using Delta C-14 in Xi'an City, China. *Atmos. Environ.* **2014**, *94*, 538–545. [CrossRef]
31. LaFranchi, B.W.; McFarlane, K.J.; Miller, J.B.; Lehman, S.J.; Phillips, C.L.; Andrews, A.E.; Tans, P.P.; Chen, H.; Liu, Z.; Turnbull, J.C.; et al. Strong regional atmospheric C-14 signature of respired CO2 observed from a tall tower over the midwestern United States. *J. Geophys. Res.-Biogeo.* **2016**, *121*, 2275–2295. [CrossRef]
32. Turnbull, J.C.; Keller, E.D.; Baisden, T.; Brailsford, G.; Bromley, T.; Norris, M.; Zondervan, A. Atmospheric measurement of point source fossil CO_2 emissions. *Atmos. Chem. Phys.* **2014**, *14*, 5001–5014. [CrossRef]
33. Karion, A.; Sweeney, C.; Tans, P.; Newberger, T. AirCore: An Innovative Atmospheric Sampling System. *J. Atmos. Ocean. Technol.* **2010**, *27*, 1839–1853. [CrossRef]
34. Paul, D.; Chen, H.; Been, H.A.; Kivi, R.; Meijer, H.A.J. Radiocarbon analysis of stratospheric CO_2 retrieved from AirCore sampling. *Atmos. Meas. Technol.* **2016**, *9*, 4997–5006. [CrossRef]
35. Hsueh, D.Y.; Krakauer, N.Y.; Randerson, J.T.; Xu, X.M.; Trumbore, S.E.; Southon, J.R. Regional patterns of radiocarbon and fossil fuel-derived CO_2 in surface air across North America. *Geophys. Res. Lett.* **2007**, *34*, L02815. [CrossRef]
36. Palstra, S.W.L.; Karstens, U.; Streurman, H.-J.; Meijer, H.A.J. Wine ethanol C-14 as a tracer for fossil fuel CO2 emissions in Europe: Measurements and model comparison. *J. Geophys. Res.-Atmos.* **2008**, *113*, D21. [CrossRef]
37. Riley, W.J.; Hsueh, D.Y.; Randerson, J.T.; Fischer, M.L.; Hatch, J.G.; Pataki, D.E.; Wang, W.; Goulden, M.L. Where do fossil fuel carbon dioxide emissions from California go? An analysis based on radiocarbon observations and an atmospheric transport model. *J Geophys. Res.-Biogeo.* **2008**, *113*, G04002. [CrossRef]
38. Park, J.H.; Hong, W.; Xu, X.; Park, G.; Sung, K.S.; Sung, K.; Lee, J.-G.; Nakanishi, T.; Park, H.-S. The distribution of Delta C-14 in Korea from 2010 to 2013. *Nucl. Instrum. Methods Phys. Res. Sect. B-Beam Interact. Mater. At.* **2015**, *361*, 609–613. [CrossRef]
39. Djuricin, S.; Xu, X.; Pataki, D.E. The radiocarbon composition of tree rings as a tracer of local fossil fuel emissions in the Los Angeles basin: 1980–2008. *J. Geophys. Res. Atmos.* **2012**, *117*. [CrossRef]
40. Hou, Y.; Zhou, W.; Cheng, P.; Xiong, X.; Du, H.; Niu, Z.; Yu, X.; Fu, Y.; Lu, X. (14)C-AMS measurements in modern tree rings to trace local fossil fuel-derived CO_2 in the greater Xi'an area, China. *Sci. Total Environ.* **2020**, *715*, 136669. [CrossRef]
41. Bozhinova, D.; van der Molen, M.K.; van der Velde, I.R.; Krol, M.C.; van der Laan, S.; Meijer, H.A.J.; Peters, W. Simulating the integrated summertime Delta(CO_2)-C-14 signature from anthropogenic emissions over Western Europe. *Atmos. Chem. Phys.* **2014**, *14*, 7273–7290. [CrossRef]
42. Bozhinova, D.; Palstra, S.W.L.; van der Molen, M.K.; Krol, M.C.; Meijer, H.A.J.; Peters, W. Three years of delta(CO_2)-C-14 observations from maize leaves in the netherlands and western europe. *Radiocarbon* **2016**, *58*, 459–478. [CrossRef]
43. Piotrowska, N.; Pazdur, A.; Pawelczyk, S.; Rakowski, A.Z.; Sensula, B.; Tudyka, K. Human activity recorded in carbon isotopic composition of atmospheric CO_2 in gliwice urban area and surroundings (southern poland) in the years 2011–2013. *Radiocarbon* **2019**, *62*, 141–156. [CrossRef]
44. Xiong, X.; Zhou, W.; Cheng, P.; Wu, S.; Niu, Z.; Du, H.; Lu, X.; Fu, Y.; Burr, G.S. Delta(CO_2)-C-14 from dark respiration in plants and its impact on the estimation of atmospheric fossil fuel CO_2. *J. Environ. Radioact.* **2017**, *169*, 79–84. [CrossRef]
45. Zhao, C.L.; Tans, P.P.; Thoning, K.W. A high precision manometric system for absolute calibrations of CO_2 in dry air. *J. Geophys. Res. Atmos.* **1997**, *102*, 5885–5894. [CrossRef]
46. Slota, P.J.; Jull, A.J.T.; Linick, T.W.; Toolin, L.J. Preparation of Small Samples for 14C Accelerator Targets by Catalytic Reduction of CO. *Radiocarbon* **1987**, *29*, 303–306. [CrossRef]
47. McNichol, A.P.; Gagnon, A.R.; Jones, G.A.; Osborne, E.A. Illumination of a Black Box: Analysis of Gas Composition During Graphite Target Preparation. *Radiocarbon* **2016**, *34*, 321–329. [CrossRef]
48. Anderson, E.C.; Arnold, J.R.; Libby, W.F. Measurement of Low Level Radiocarbon. *Rev. Sci. Instrum.* **1951**, *22*, 225–230. [CrossRef] [PubMed]
49. Litherland, A.E. Ultrasensitive Mass Spectrometry with Accelerators. *Annu. Rev. Nucl. Part Sci.* **1980**, *30*, 437–473. [CrossRef]
50. Ziolkowski, L.A.; Druffel, E.R. Quantification of extraneous carbon during compound specific radiocarbon analysis of black carbon. *Anal. Chem.* **2009**, *81*, 10156–10161. [CrossRef]
51. Smith, A.M.; Hua, Q.; Williams, A.; Levchenko, V.; Yang, B. Developments in micro-sample 14C AMS at the ANTARES AMS facility. *Nucl. Instrum. Methods Phys. Res. Sect. B Beam Interact. Mater. At.* **2010**, *268*, 919–923. [CrossRef]
52. Turnbull, J.; Mikaloff Fletcher, S.E.; Ansell, I.; Brailsford, G.; Moss, R.; Norris, M.; Steinkamp, K. Sixty years of radiocarbon dioxide measurements at Wellington, New Zealand: 1954–2014. *Atmos. Chem. Phys.* **2017**, *17*, 14771–14784. [CrossRef]
53. Levin, I.; Kromer, B.; Hammer, S. Atmospheric Δ14CO2 trend in Western European background air from 2000 to 2012. *Tellus B Chem. Phys. Meteorol.* **2013**, *65*, 20092. [CrossRef]
54. Graven, H.D.; Guilderson, T.P.; Keeling, R.F. Observations of radiocarbon in CO2 at La Jolla, California, USA 1992-2007: Analysis of the long-term trend. *J. Geophys. Res.-Atmos.* **2012**, *117*, D02302. [CrossRef]

55. Lehman, S.J.; Miller, J.B.; Wolak, C.; Southon, J.; Tans, P.P.; Montzka, S.A.; Sweeney, C.; Andrews, A.; LaFranchi, B.; Guilderson, T.P.; et al. Allocation of terrestrial carbon sources using (CO_2)-C-14: Methods, measurement, and modeling. *Radiocarbon* **2013**, *55*, 1484–1495. [CrossRef]
56. Turnbull, J.; Lehman, S.J.; Miller, J.B.; Sparks, R.J.; Southon, J.R.; Tans, P.P. A new high precision14CO2 time series for North American continental air. *J. Geophys. Res.* **2007**, *112*, D11310. [CrossRef]
57. Niu, Z.; Zhou, W.; Cheng, P.; Wu, S.; Lu, X.; Xiong, X.; Du, H.; Fu, Y. Observations of Atmospheric Delta(CO_2)-C-14 at the Global and Regional Background Sites in China: Implication for Fossil Fuel CO_2 Inputs. *Environ. Sci. Technol.* **2016**, *50*, 12122–12128. [CrossRef] [PubMed]
58. Turnbull, J.; Tans, P.P.; Lehman, S.J.; Baker, D.; Conway, T.J.; Chung, Y.S.; Gregg, J.; Miller, J.B.; Southon, J.R.; Zhou, L.-X. Atmospheric observations of carbon monoxide and fossil fuel CO2 emissions from East Asia. *J. Geophys. Res.-Atmos.* **2011**, *116*, D24306. [CrossRef]
59. Levin, I.; Hammer, S.; Kromer, B.; Meinhardt, F. Radiocarbon observations in atmospheric CO2: Determining fossil fuel CO2 over Europe using Jungfraujoch observations as background. *Sci. Total Environ.* **2008**, *391*, 211–216. [CrossRef]
60. Schmidt, M.; Graul, R.; Sartorius, H.; Levin, I. The Schauinsland CO_2 record: 30 years of continental observations and their implications for the variability of the European CO_2 budget. *J. Geophys. Res.* **2003**, 108. [CrossRef]
61. Currie, K.I.; Brailsford, G.; Nichol, S.; Gomez, A.; Sparks, R.; Lassey, K.R.; Riedel, K. Tropospheric 14CO_2 at Wellington, New Zealand: The world's longest record. *Biogeochemistry* **2011**, *104*, 5–22. [CrossRef]
62. Patra, P.K.; Houweling, S.; Krol, M.; Bousquet, P.; Belikov, D.; Bergmann, D.; Bian, H.; Cameron-Smith, P.; Chipperfield, M.P.; Corbin, K.; et al. TransCom model simulations of CH_4 and related species: Linking transport, surface flux and chemical loss with CH4 variability in the troposphere and lower stratosphere. *Atmos. Chem. Phys.* **2011**, *11*, 12813–12837. [CrossRef]
63. Graven, H.D. Impact of fossil fuel emissions on atmospheric radiocarbon and various applications of radiocarbon over this century. *Proc. Natl. Acad. Sci. USA* **2015**, *112*, 9542–9545. [CrossRef]
64. Wang, R.; Tao, S.; Ciais, P.; Shen, H.Z.; Huang, Y.; Chen, H.; Shen, G.F.; Wang, B.; Li, W.; Zhang, Y.Y.; et al. High-resolution mapping of combustion processes and implications for CO_2 emissions. *Atmos. Chem. Phys.* **2013**, *13*, 5189–5203. [CrossRef]
65. Molnar, M.; Haszpra, L.; Svingor, E.; Major, I.; Svetlik, I. Atmospheric fossil fuel CO_2 measurement using a field unit in a central european city during the winter of 2008/09. *Radiocarbon* **2010**, *52*, 835–845. [CrossRef]
66. Molnar, M.; Major, I.; Haszpra, L.; Svetlik, I.; Svingor, E.; Veres, M. Fossil fuel CO_2 estimation by atmospheric C-14 measurement and CO_2 mixing ratios in the city of Debrecen, Hungary. *J. Radioanal. Nucl. Chem.* **2010**, *286*, 471–476. [CrossRef]
67. Faurescu, I.; Varlam, C.; Vagner, I.; Faurescu, D.; Bogdan, D.; Costinel, D. Radiocarbon level in the atmosphere of ramnicu valcea, romania. *Radiocarbon* **2019**, *61*, 1625–1632. [CrossRef]
68. Wenger, A.; Pugsley, K.; O'Doherty, S.; Rigby, M.; Manning, A.J.; Lunt, M.F.; White, E.D. Atmospheric radiocarbon measurements to quantify CO2 emissions in the UK from 2014 to 2015. *Atmos. Chem. Phys.* **2019**, *19*, 14057–14070. [CrossRef]
69. Newman, S.; Xu, X.; Gurney, K.R.; Hsu, Y.K.; Li, K.F.; Jiang, X.; Keeling, R.; Feng, S.; O'Keefe, D.; Patarasuk, R.; et al. Toward consistency between trends in bottom-up CO_2 emissions and top-down atmospheric measurements in the Los Angeles megacity. *Atmos. Chem. Phys.* **2016**, *16*, 3843–3863. [CrossRef]
70. Vay, S.A.; Choi, Y.; Vadrevu, K.P.; Blake, D.R.; Tyler, S.C.; Wisthaler, A.; Hecobian, A.; Kondo, Y.; Diskin, G.S.; Sachse, G.W.; et al. Patterns of CO2 and radiocarbon across high northern latitudes during International Polar Year 2008. *J. Geophys. Res.-Atmos.* **2011**, *116*, D14301. [CrossRef]
71. Cui, X.; Newman, S.; Xu, X.; Andrews, A.E.; Miller, J.; Lehman, S.; Jeong, S.; Zhang, J.; Priest, C.; Campos-Pineda, M.; et al. Atmospheric observation-based estimation of fossil fuel CO_2 emissions from regions of central and southern California. *Sci. Total Environ.* **2019**, *664*, 381–391. [CrossRef]
72. 7Vay, S.A.; Tyler, S.C.; Choi, Y.; Blake, D.R.; Blake, N.J.; Sachse, G.W.; Diskin, G.S.; Singh, H.B. Sources and transport of delta C-14 in CO_2 within the Mexico City Basin and vicinity. *Atmos. Chem. Phys.* **2009**, *9*, 4973–4985. [CrossRef]
73. Park, J.H.; Hong, W.; Park, G.; Sung, K.S.; Lee, K.H.; Kim, Y.E.; Kim, J.K.; Choi, H.W.; Kim, G.D.; Woo, H.J. Distributions of fossil fuel originated CO2 in five metropolitan areas of Korea (Seoul, Busan, Daegu, Daejeon, and Gwangju) according to the Delta C-14 in ginkgo leaves. *Nucl. Instrum. Methods Phys. Res. Sect. B-Beam Interact. Mater. At.* **2013**, *294*, 508–514. [CrossRef]
74. Niu, Z.; Zhou, W.; Zhang, X.; Wang, S.; Zhang, D.; Lu, X.; Cheng, P.; Wu, S.; Xiong, X.; Du, H.; et al. The spatial distribution of fossil fuel CO2 traced by Delta C-14 in the leaves of gingko (Ginkgo biloba L.) in Beijing City, China. *Environ. Sci. Pollut. R* **2016**, *23*, 556–562. [CrossRef]
75. Xi, X.T.; Ding, X.F.; Fu, D.P.; Zhou, L.P.; Liu, K.X. Regional Delta C-14 patterns and fossil fuel derived CO2 distribution in the Beijing area using annual plants. *Chin. Sci. Bull.* **2011**, *56*, 1721–1726. [CrossRef]
76. Niu, Z.; Zhou, W.; Wu, S.; Cheng, P.; Lu, X.; Xiong, X.; Du, H.; Fu, Y.; Wang, G. Atmospheric Fossil Fuel CO_2 Traced by Delta C-14 in Beijing and Xiamen, China: Temporal Variations, Inland/Coastal Differences and Influencing Factors. *Environ. Sci. Technol.* **2016**, *50*, 5474–5480. [CrossRef] [PubMed]
77. Ding, P.; Shen, C.D.; Yi, W.X.; Wang, N.; Ding, X.F.; Fu, D.P.; Liu, K.X. Fossil-fuel-derived CO_2 contribution to the urban atmosphere in guangzhou, south china, estimated by (CO2)-C-14 observation, 2010–2011. *Radiocarbon* **2013**, *55*, 791–803. [CrossRef]
78. Xiong, X.H.; Zhou, W.J.; Wu, S.G.; Cheng, P.; Du, H.; Hou, Y.Y.; Niu, Z.C.; Wang, P.; Lu, X.F.; Fu, Y.C. Two-Year Observation of Fossil Fuel Carbon Dioxide Spatial Distribution in Xi'an City. *Adv. Atmos. Sci.* **2020**, *37*, 569–575. [CrossRef]

79. Zhou, W.; Niu, Z.; Wu, S.; Xiong, X.; Hou, Y.; Wang, P.; Feng, T.; Cheng, P.; Du, H.; Lu, X.; et al. Fossil fuel CO_2 traced by radiocarbon in fifteen Chinese cities. *Sci. Total Environ.* **2020**, 729. [CrossRef]
80. Wang, P.; Zhou, W.; Niu, Z.; Cheng, P.; Wu, S.; Xiong, X.; Lu, X.; Du, H. Emission characteristics of atmospheric carbon dioxide in Xi'an, China based on the measurements of CO2 concentration, big up tri, open(14)C and delta(13)C. *Sci. Total Environ.* **2018**, *619–620*, 1163–1169. [CrossRef]
81. Varga, T.; Jull, A.J.T.; Lisztes-Szabó, Z.; Molnár, M. Spatial Distribution of 14C in Tree Leaves from Bali, Indonesia. *Radiocarbon* **2019**, *62*, 235–242. [CrossRef]
82. Park, J.H.; Hong, W.; Park, G.; Sung, K.S.; Lee, K.H.; Kim, Y.E.; Kim, J.K.; Choi, H.W.; Kim, G.D.; Woo, H.J.; et al. A comparison of distribution maps of Delta C-14 in 2010 and 2011 in korea. *Radiocarbon* **2013**, *55*, 841–847. [CrossRef]
83. Xi, X.T.; Ding, X.F.; Fu, D.P.; Zhou, L.P.; Liu, K.X. Delta C-14 level of annual plants and fossil fuel derived CO2 distribution across different regions of China. *Nucl. Instrum. Methods Phys. Res. Sect. B-Beam Interact. Mater. At.* **2013**, *294*, 515–519. [CrossRef]
84. Feng, T.; Zhou, W.; Wu, S.; Niu, Z.; Cheng, P.; Xiong, X.; Li, G. Simulations of summertime fossil fuel CO_2 in the Guanzhong basin, China. *Sci. Total Environ.* **2018**, *624*, 1163–1170. [CrossRef]
85. Wu, S.G.; Zhou, W.J.; Cheng, P.; Xiong, X.H.; Zhou, J.; Feng, T.; Hou, Y.Y.; Chen, N.; Wang, P.; Du, H.; et al. Tracing fossil fuel CO_2 by C-14 in maize leaves in Guanzhong Basin of China. *J Environ. Manag.* **2022**, *323*, 116286. [CrossRef] [PubMed]
86. Turnbull, J.; Miller, J.B.; Lehman, S.J.; Hurst, D.; Peters, W.; Tans, P.P.; Southon, J.; Montzka, S.A.; Elkins, J.W.; Mondeel, D.J.; et al. Spatial distribution of Delta(CO2)-C-14 across Eurasia: Measurements from the TROICA-8 expedition. *Atmos. Chem. Phys.* **2009**, *9*, 175–187. [CrossRef]
87. Levin, I.; Hammer, S.; Eichelmann, E.; Vogel, F.R. Verification of greenhouse gas emission reductions: The prospect of atmospheric monitoring in polluted areas. *Philos Trans. R. Soc. A* **2011**, *369*, 1906–1924. [CrossRef] [PubMed]
88. Niu, Z.; Zhou, W.; Feng, X.; Hou, Y.; Chen, N.; Du, H.; Wu, S.; Fu, Y.; Lu, X.; Cheng, P.; et al. Determining diurnal fossil fuel CO_2 and biological CO_2 by Delta(CO_2)-C-14 observation on certain summer and winter days at Chinese background sites. *Sci. Total Environ.* **2020**, 718. [CrossRef]
89. Wang, P.; Zhou, W.J.; Niu, Z.C.; Xiong, X.H.; Wu, S.G.; Cheng, P.; Hou, Y.Y.; Lu, X.F.; Du, H. Spatio-temporal variability of atmospheric CO_2 and its main causes: A case study in Xi'an city, China. *Atmos. Res.* **2021**, 249. [CrossRef]
90. Zimnoch, M.; Jelen, D.; Galkowski, M.; Kuc, T.; Necki, J.; Chmura, L.; Gorczyca, Z.; Jasek, A.; Rozanski, K. Partitioning of atmospheric carbon dioxide over Central Europe: Insights from combined measurements of CO_2 mixing ratios and their carbon isotope composition. *Isot. Environ. Health Stud.* **2012**, *48*, 421–433. [CrossRef]
91. Bozhinova, D.; Combe, M.; Palstra, S.W.L.; Meijer, H.A.J.; Krol, M.C.; Peters, W. The importance of crop growth modeling to interpret the Delta(CO_2)-C-14 signature of annual plants. *Glob. Biogeochem. Cycles* **2013**, *27*, 792–803. [CrossRef]
92. Andres, R.J.; Boden, T.A.; Higdon, D. A new evaluation of the uncertainty associated with CDIAC estimates of fossil fuel carbon dioxide emission. *Tellus B Chem. Phys. Meteorol.* **2014**, *66*, 23616. [CrossRef]
93. Liu, Z.; Guan, D.; Wei, W.; Davis, S.J.; Ciais, P.; Bai, J.; Peng, S.; Zhang, Q.; Hubacek, K.; Marland, G.; et al. Reduced carbon emission estimates from fossil fuel combustion and cement production in China. *Nature* **2015**, *524*, 335–338. [CrossRef]
94. Han, P.; Zeng, N.; Oda, T.; Lin, X.; Crippa, M.; Guan, D.; Janssens-Maenhout, G.; Ma, X.; Liu, Z.; Shan, Y.; et al. Evaluating China's fossil-fuel CO_2 emissions from a comprehensive dataset of nine inventories. *Atmos. Chem. Phys.* **2020**, *20*, 11371–11385. [CrossRef]
95. Göckede, M.; Michalak, A.M.; Vickers, D.; Turner, D.P.; Law, B.E. Atmospheric inverse modeling to constrain regional-scale CO_2 budgets at high spatial and temporal resolution. *J. Geophys. Res.* **2010**, 115. [CrossRef]
96. Lauvaux, T.; Miles, N.L.; Deng, A.; Richardson, S.J.; Cambaliza, M.O.; Davis, K.J.; Gaudet, B.; Gurney, K.R.; Huang, J.; O'Keefe, D.; et al. High-resolution atmospheric inversion of urban CO_2 emissions during the dormant season of the Indianapolis Flux Experiment (INFLUX). *J. Geophys. Res. Atmos.* **2016**, *121*, 5213–5236. [CrossRef] [PubMed]
97. Evangeliou, N.; Thompson, R.L.; Eckhardt, S.; Stohl, A. Top-down estimates of black carbon emissions at high latitudes using an atmospheric transport model and a Bayesian inversion framework. *Atmos. Chem. Phys.* **2018**, *18*, 15307–15327. [CrossRef]
98. Hedelius, J.K.; Liu, J.J.; Oda, T.; Maksyutov, S.; Roehl, C.M.; Iraci, L.T.; Podolske, J.R.; Hillyard, P.W.; Liang, J.M.; Gurney, K.R.; et al. Southern California megacity CO_2, CH_4, and CO flux estimates using ground- and space-based remote sensing and a Lagrangian model. *Atmos. Chem. Phys.* **2018**, *18*, 16271–16291. [CrossRef]
99. Turnbull, J.C.; Keller, E.D.; Norris, M.W.; Wiltshire, R.M. Independent evaluation of point source fossil fuel CO_2 emissions to better than 10%. *Proc. Natl. Acad. Sci. USA* **2016**, *113*, 10287–10291. [CrossRef] [PubMed]
100. Basu, S.; Miller, J.B.; Lehman, S. Separation of biospheric and fossil fuel fluxes of CO_2 by atmospheric inversion of CO_2 and (CO_2)-C-14 measurements: Observation System Simulations. *Atmos. Chem. Phys.* **2016**, *16*, 5665–5683. [CrossRef]
101. Wang, Y.; Broquet, G.; Ciais, P.; Chevallier, F.; Vogel, F.; Kadygrov, N.; Wu, L.; Yin, Y.; Wang, R.; Tao, S. Estimation of observation errors for large-scale atmospheric inversion of CO2 emissions from fossil fuel combustion. *Tellus Ser. B-Chem. Phys. Meteorol.* **2017**, *69*. [CrossRef]
102. Potier, E.; Broquet, G.; Wang, Y.L.; Santaren, D.; Berchet, A.; Pison, I.; Marshall, J.; Ciais, P.; Breon, F.M.; Chevallier, F. Complementing XCO_2 imagery with ground-based CO_2 and (CO_2)-C-14 measurements to monitor CO_2 emissions from fossil fuels on a regional to local scale. *Atmos. Meas. Technol.* **2022**, *15*, 5261–5288. [CrossRef]
103. Levin, I.; Worthy, D.E.J. Implications for Deriving Regional Fossil Fuel CO_2 Estimates from Atmospheric Observations in a Hot Spot of Nuclear Power Plant $14CO_2$ Emissions. *Radiocarbon* **2016**, *55*, 1556–1572. [CrossRef]

104. Graven, H.D.; Gruber, N. Continental-scale enrichment of atmospheric (CO_2)-C-14 from the nuclear power industry: Potential impact on the estimation of fossil fuel-derived CO_2. *Atmos. Chem. Phys.* **2011**, *11*, 12339–12349. [CrossRef]
105. Kuderer, M.; Hammer, S.; Levin, I. The influence of (CO_2)-C-14 releases from regional nuclear facilities at the Heidelberg (CO_2)-C-14 sampling site (1986–2014). *Atmos. Chem. Phys.* **2018**, *18*, 7951–7959. [CrossRef]
106. Wang, P.; Zhou, W.J.; Xiong, X.H.; Wu, S.G.; Niu, Z.C.; Yu, Y.L.; Liu, J.Z.; Feng, T.; Cheng, P.; Du, H.; et al. Source Attribution of Atmospheric CO2 Using C-14 and C-13 as Tracers in Two Chinese Megacities During Winter. *J. Geophys. Res.-Atmos.* **2022**, *127*, 1–12. [CrossRef]